Materials Horizons

ROYAL SOCIETY OF CHEMISTRY

COMMUNICATION

Check for updates

Cite this: *Mater. Horiz.*, 2020, 7, 2359

Received 12th May 2020, Accepted 8th June 2020

DOI: 10.1039/d0mh00787k

rsc.li/materials-horizons

Machine-learning interatomic potentials enable first-principles multiscale modeling of lattice thermal conductivity in graphene/borophene heterostructures†

Bohayra Mortazavi, *[ab] Evgeny V. Podryabinkin,[c] Stephan Roche,[de] Timon Rabczuk,[f] Xiaoying Zhuang*[af] and Alexander V. Shapeev[c]

One of the ultimate goals of computational modeling in condensed matter is to be able to accurately compute materials properties with minimal empirical information. First-principles approaches such as density functional theory (DFT) provide the best possible accuracy on electronic properties but they are limited to systems up to a few hundreds, or at most thousands of atoms. On the other hand, classical molecular dynamics (CMD) simulations and the finite element method (FEM) are extensively employed to study larger and more realistic systems, but conversely depend on empirical information. Here, we show that machine-learning interatomic potentials (MLIPs) trained over short *ab initio* molecular dynamics trajectories enable first-principles multiscale modeling, in which DFT simulations can be hierarchically bridged to efficiently simulate macroscopic structures. As a case study, we analyze the lattice thermal conductivity of coplanar graphene/borophene heterostructures, recently synthesized experimentally (*Sci. Adv.*, 2019, 5, eaax6444), for which no viable classical modeling alternative is presently available. Our MLIP-based approach can efficiently predict the lattice thermal conductivity of graphene and borophene pristine phases, the thermal conductance of complex graphene/borophene interfaces and subsequently enable the study of effective thermal transport along the heterostructures at continuum level. This work highlights that MLIPs can be effectively and conveniently employed to enable first-principles multiscale modeling *via* hierarchical employment of DFT/CMD/FEM simulations, thus expanding the capability for computational design of novel nanostructures.

New concepts

This study highlights that machine-learning interatomic potentials (MLIPs) trained over *ab initio* molecular dynamics trajectories enable the design of an efficient first-principles multiscale modeling, branching density functional theory with classical molecular dynamics and finite element simulations. Thanks to such methodology, it becomes possible to examine the properties and responses of structurally complex microstructures and assemblies, with the precision of sophisticated first principles calculations, without paying its corresponding computational cost.

From the engineering point of view, numerical modeling is currently a fundamental aspect of structural design, which not only substantially reduces the final costs of a product but also enables the optimization toward the improved performance. However, before conducting an engineering simulation, materials properties are ought to be evaluated accurately. In comparison with conventional materials, experimental techniques for the characterization of nanomaterials properties are substantially more complicated, time-consuming and expensive as well. More importantly, for nanomaterials the experimentally reported properties may show considerable scatterings, stemming from diverse sources of uncertainties in the measurements. Like other engineering products, for the practical application of nanomaterials in various technologies, developments of accurate modeling

---

[a] Chair of Computational Science and Simulation Technology, Department of Mathematics and Physics, Leibniz Universität Hannover, Appelstraße 11, 30157 Hannover, Germany. E-mail: bohayra.mortazavi@gmail.com

[b] Cluster of Excellence PhoenixD (Photonics, Optics, and Engineering-Innovation Across Disciplines), Gottfried Wilhelm Leibniz Universität Hannover, Hannover, Germany

[c] Skolkovo Institute of Science and Technology, Skolkovo Innovation Center, Nobel St. 3, Moscow 143026, Russia

[d] Catalan Institute of Nanoscience and Nanotechnology (ICN2), CSIC and BIST, Campus UAB, Bellaterra, 08193 Barcelona, Spain

[e] ICREA Institució Catalana de Recerca i Estudis Avancats, 08010 Barcelona, Spain

[f] College of Civil Engineering, Department of Geotechnical Engineering, Tongji University, Shanghai, China. E-mail: zhuang@ikm.uni-hannover.de

† Electronic supplementary information (ESI) available: The Supplementary Information document with computational details is available to download at http://dx.doi.org/10.17632/pbgscy3ptg.1. It contains the details of the computations, geometry optimized graphene/borophene heterostructures, examples of untrained MTPs, examples of VASP input parameters for the AIMD simulations, an example of non-equilibrium molecular dynamics simulation of thermal conductance with the MTP to introduce the atomic interactions using the LAMMPS package and developed codes to employ the MTPs for acquiring the anharmonic force constants for the BTE solution using the ShengBTE package, and the created input files for the ShengBTE solution of the lattice thermal conductivity of graphene, silicon and InAs. See DOI: 10.1039/d0mh00787k

approaches are critical to facilitate the design and further optimizations. In recent years theoretical simulations have played a major role in the astonishing advances in the field of materials science. In this regard, modeling enables researchers to examine the stability and explore the properties of novel materials and structures purely through computer simulations. Notably, first-principles simulations can already be employed to find possible synthesis routes for the design of novel materials.[1–3] As a recent example, boron nanosheets with different atomic lattices were epitaxially grown over the silver surface,[4,5] a fabrication process that was originally proposed by the density functional theory (DFT) simulations.[6,7]

The main drawback of first-principles DFT calculations is nonetheless related to their demanding computational cost, which limits the maximal size of studied systems to only several hundreds, or at most a few thousand atoms. Moreover, the computational costs of common DFT simulations normally scale exponentially with the number of atoms, which jeopardize the numerical exploration of large and disordered material models such as the amorphous graphene.[8] Classical molecular dynamics (CMD) simulation is also among the most popular numerical approaches, and has been extensively employed to explore the properties of complex nanostructured materials. Unlike DFT simulations, the computational cost of CMD calculations scales linearly with the number of atoms, giving access to million-atom scale modeling. However, the accuracy of CMD results strongly depends on the precision of the interatomic potentials in describing energies and forces. As a well-known example, despite the rather simple bonding mechanism in the planar full-sp^2 carbon system, most of the currently available interatomic potentials cannot accurately reproduce the thermal conductivity of graphene. Additionally, for novel materials and structures, it is a challenging task to find an interatomic potential that maintains structural stability, irrespective of the accuracy in estimating the basic mechanical or vibrational properties. It is clear that in comparison with the DFT counterpart, the computational advantage of MD simulations comes with the costs of declined accuracy. On the other side, continuum mechanic based method like the finite element method (FEM) offer robust solutions to study practical engineering problems, but in these methods, the properties of the materials should be fully known prior to launching a simulation. It is thus conspicuous that for studying the properties and responses of nanomaterials, the development of multiscale approaches, solving each method's drawback, is crucially needed.

The latest advances in the field of machine-learning methods have offered novel solutions to address critical challenges for a number of problems, especially in materials science.[9–12] For example, as discussed in numerous studies[13–19] machine-learning techniques are expected to revolutionize the materials discovery and design. One of the latest advances in this regard, is the use of machine-learning interatomic potentials (MLIPs) to substantially enhance the accuracy of CMD simulations. Recently, MLIPs have been successfully employed to predict novel materials[20,21] and examine lattice dynamics[22,23] and thermal conductivity.[24,25] As proven in numerous recent studies,[22,24,26] MLIPs enable CMD simulations to be conducted within the DFT level accuracy for the computed energies and forces, but with computational costs scaling linearly with the number of atoms. Another remarkable advantage of MLIPs is that being derived from DFT simulations, they can be trained for a specific material composition and are thus less affected by the flexibility issue of standard CMD method. Accordingly, MLIPs offer unprecedented possibility to marry first-principles accuracy with multiscale modeling. To illustrate such strategy, here we examine the lattice thermal conductivity of graphene/borophene heterostructures,[27] as a truly challenging system to simulate accurately with conventional methods. To date, there is no available classical interatomic potential that can accurately reproduce the structural properties of borophene and borophene/graphene nanosheets. Moreover, for a well-studied system like graphene, while the majority of interatomic potentials provide structural and elastic constants with a sufficient accuracy, when applied to the calculation of the lattice thermal conductivity, variation of one order of magnitude is observed. For the case of graphene, the experimentally measured thermal conductivities lie in the range 1500–5300 W mK^{-1},[28–31] while CMD based estimates by the original Tersoff,[32] AIREBO,[33] REBO[34] and optimized Tersoff[35] give values of 870,[36] 709,[37] 350[38] and $\sim$3000 W mK^{-1},[39,40] respectively. Accordingly it is evident that the prediction of lattice thermal conductivity using classical interatomic potential remains a highly challenging task. In addition, when using CMD simulations to evaluate the interfacial thermal conductance, the interatomic potential must exhibit both high stability and accuracy, otherwise the calculations fail to simulate the steady-state heat transfer.[41–43] Therefore the stability of simulations is a critical issue for the modeling of graphene/borophene structures, not only because of their different lattices but also due to the possibility of formation of diverse types of defects at their interface.

The main steps within the first-principles hierarchical multiscale modeling framework proposed here are summarized in Fig. 1. This includes four key steps: (1) DFT simulations; (2) development of MLIPs; (3) CMD simulations and (4) FEM modeling of effective lattice thermal conductivity. Within the DFT step, we first conduct the energy minimization of graphene and borophene lattices. Next, ten different possible grain boundaries (GBs) between the graphene and borophene lattices (find Fig. 2a) are studied. Since we conduct the DFT simulations within the plane-wave approach, the constructed models are periodic in planar directions, so that it is possible to construct two different grain boundaries in every DFT interface model (see Section 2 in the ESI†). To create the required training sets for the development of MLIPs, *ab initio* molecular dynamics (AIMD) simulations are performed. These simulations are carried out for pristine phases (pure graphene or borophene) and heterostructures with geometry optimized interfaces at different temperatures of 100, 300, 600 and 700 K, each one with less than 1000 time steps. Since the AIMD trajectories are correlated within short time periods, only every 10th steps of the original trajectories are included in the training sets. Next, moment tensor potentials (MTPs)[44] are parameterized to describe the interatomic interactions. Similarly to classical counterparts, MTPs also include parameters which are optimized over the

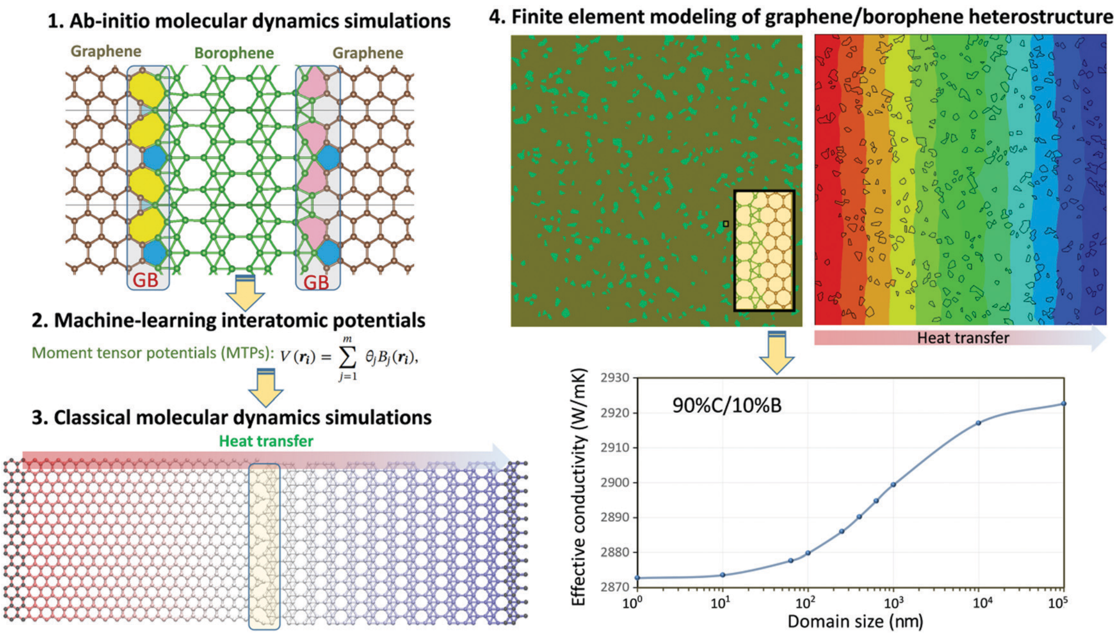
1. Ab-initio molecular dynamics simulations
Graphene
Borophene
Graphene
GB
GB
2. Machine-learning interatomic potentials
Moment tensor potentials (MTPs): $V(\boldsymbol{r}_i)=\sum_{j=1}^{m}\theta_j B_j(\boldsymbol{r}_i)$,
3. Classical molecular dynamics simulations
Heat transfer
4. Finite element modeling of graphene/borophene heterostructures
Heat transfer
90%C/10%B
Effective conductivity (W/mK)
2930
2920
2910
2900
2890
2880
2870
10^0
10^1
10^2
10^3
10^4
10^5
Domain size (nm)

Fig. 1 Main steps of the proposed first-principles multiscale modeling framework to simulate the lattice thermal conductivity of graphene/borophene heterostructures.

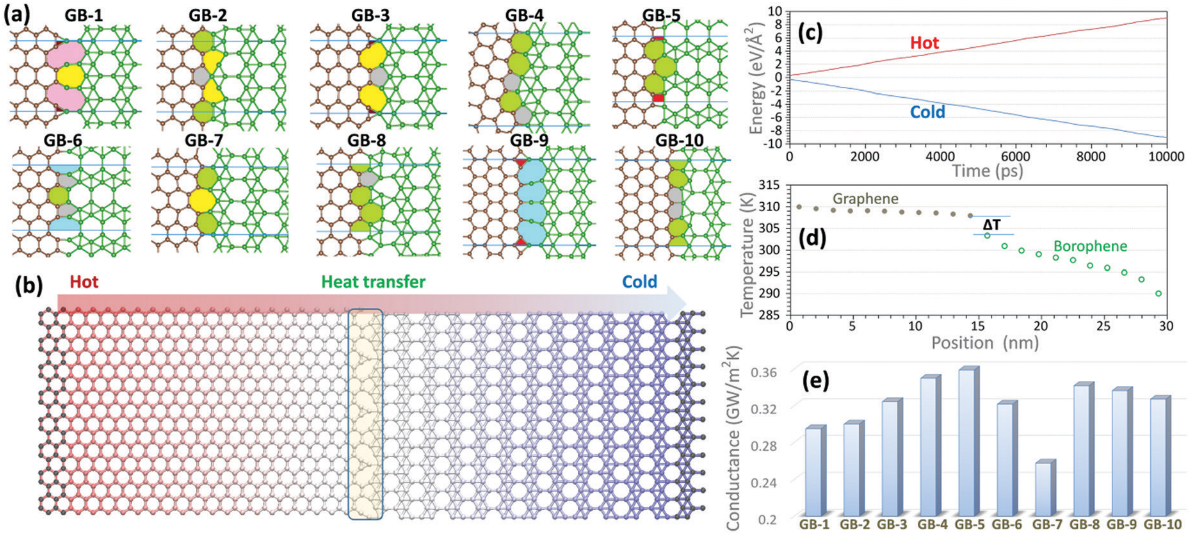

Fig. 2 (a) Atomic configurations of constructed graphene/borophene grain boundaries (GB), (b) schematic illustration of non-equilibrium molecular dynamics (NEMD) method, (c) energy values added to the hot slab and removed from the cold slab by the *NVT* thermostat during every simulation time step, (d) established temperature profile showing a sudden drop at the interface (e) estimated interfacial thermal conductance of considered grain boundaries in panel (a).

training configurations provided by the AIMD simulations. In this work, two types of MTPs are developed, mono-elemental potentials to simulate the pristine graphene or borophene and binary potentials for the heterostructure samples. In the latter case, the created training sets not only include the AIMD trajectories from the constructed heterostructures but also those from the pristine graphene and borophene lattices. For the computational efficiency, MTPs are first trained over subsampled AIMD trajectories. After the preliminary training of MTPs, the accuracy of the trained potentials is evaluated over the full AIMD trajectories and the configurations with high extrapolations grades[26] are identified. Such selected configurations are then added to the original training sets and the final MTPs developed by retraining the updated clean potentials over the updated training sets (see Section 1 in the ESI†). After the MTPs are trained, they are used in the third step to evaluate the thermal conductivity of pristine phases or calculate the interfacial thermal conductance of grain boundaries *via* CMD simulations. In the last step, the effective lattice thermal conductivity is evaluated with the FEM method, using the input data provided by the third step.

In Fig. 2a, the atomic configurations of ten different graphene/borophene grain boundaries constructed in this study are illustrated. In this work, six different graphene and borophene heterostructure models are constructed, and from those models ten different grain boundaries are selected for the CMD simulations (find Fig. S1, ESI†). We remind that from a theoretical point of view, the grain boundaries in graphene are made from a series of pentagon/heptagon pairs.[45] For the case of MoS_2, which also shows the hexagonal unit cell, according to high-resolution electron microscopy results, grain boundaries however contain diverse forms of pentagon–heptagon (5–7), tetragon–tetragon (4–4), tetragon–hexagon (4–6), tetragon–octagon (4–8) and hexagon–octagon (6–8) rings.[46–48] Because of the different atomic lattices of borophene and graphene and depending on the various tilting angles, graphene/borophene grain boundaries show diverse configurations. From the constructed grain boundaries shown in Fig. 2a it is clear that they mainly include tetragon, pentagon, hexagon and octagon dislocations, but nonagon rings may also form as found in the case of GB-1. Non-equilibrium molecular dynamics (NEMD) simulations are then performed to access the interfacial thermal conductance and lattice thermal conductivity of pristine borophene. To this end we used the LAMMPS[49] package along with the trained MTPs to introduce the atomic interactions. In Table S1 (ESI†), we examine the accuracy of the trained MTPs for the graphene/borophene interfaces over additional 4 ps of AIMD trajectories at 300 K. Our analysis over the AIMD testing data reveals that the errors in the absolute energy of the systems are in the order of a few meV, confirming the high accuracy of the trained MTPs. In the NEMD approach periodic boundary conditions are applied along the planar directions using a simulation time step of 0.5 fs. As shown schematically in Fig. 2b, to simulate the steady-state heat transfer, we first relax the structures at room temperature using the Nosé–Hoover thermostat (*NVT*) method. Then a few rows of atoms at the two ends were fixed and the rest of the simulation box is divided into 22 slabs. Next a temperature difference of 20 K is applied between the first (hot) and last (cold) slabs. In this process, the desired temperatures at the two ends are controlled by the *NVT* method, while the remaining of the system is simulated without applying a thermostat. As shown in Fig. 2c for a sample of grain boundaries, to keep the applied temperature difference at every simulation time step an amount of energy is added to the hot slab and another amount of energy is removed from the cold slab by the *NVT* thermostat. As can be seen from Fig. 2c, the amounts of the energy added and removed to the system remain under control (that show linear patterns), confirming that the system stays under steady-state heat transfer condition. The slope of these energy curves can be used to calculate the applied steady-state heat flux (H_f). As shown in Fig. 2d, due to the existence of grain boundary, the temperature profile exhibits a sudden change at the interface (ΔT). It is noticeable that temperature gradient within the graphene region is negligible as compared with the borophene section, suggesting a considerably higher lattice thermal conductivity of graphene. The grain boundary thermal conductance can be calculated as $H_f/\Delta T$. For the pristine borophene, the temperature profile however illustrates a constant gradient, which can be used to estimate the thermal conductivity using the one-dimensional form of the Fourier law. In Fig. 2e, the calculated interfacial thermal conductance for the considered grain boundaries are compared. Notably, the thermal conductances of different grain boundaries are close. We also examine the length dependence and found that it does not affect the estimated thermal conductance, in agreement with a recent study on polycrystalline MoS_2[50] and graphene/h-BN heterostructures.[51] These observations reveal that the interfacial thermal resistance mainly stems from the very different phonon dispersion relations of graphene and borophene (find Fig. S2, ESI†), in contrast with those of polycrystalline sheets in which the misorientation angle of adjacent sheets and density and type of dislocations cores play the critical role.[50,51] Since the thermal conductance does not show substantial dependence on the geometries of the formed defects at graphene/borophene interfaces, it is thus expected that including more extensive grain boundary configurations should not lead to considerable changes in the estimated effective lattice thermal conductivity of heterostructures.

The length effect on the NEMD predictions for the lattice thermal conductivity of borophene monolayer at room temperature is plotted in Fig. 3a. Unlike the graphene, borophene shows anisotropic transport properties and therefore the calculations are conducted along the armchair and zigzag directions. Sharp initial increases in the predicted lattice thermal conductivities by increasing the sample length are observable. This length effect on the thermal conductivities suppresses at higher lengths and finally converges and reaches the diffusive heat transfer regime. As a common approach, the thermal conductivity of borophene at infinite length, k_∞, can be calculated by an extrapolation of the NEMD results for the samples with finite lengths, k_L, using the first-order rational curve fitting *via* $1/k_L = (1 + \Lambda/L)/k_\infty$,[52,53] where Λ is the effective phonon mean free path. By assuming the thickness of 2.9 Å, the diffusive lattice thermal conductivity of borophene at room temperature along with the armchair and zigzag directions were estimated to be 52 and 112 W mK^{-1}, respectively.

Another alternative to calculate the lattice thermal conductivity is to solve the Boltzmann transport equation. To that end we use the ShengBTE[60] package, which offers a full-iterative solution of the Boltzmann transport equation to estimate the lattice thermal conductivity. The computationally demanding section of aforementioned approach is to acquire the third-order (anharmonic) interatomic force constants, which usually requires a few hundred or thousand single-point DFT calculations over supercell lattices. In this work, second and third-order force constants are calculated using the density functional perturbation theory simulations and passively trained MTPs, respectively, over $10 \times 10 \times 1$ super-cells (consisting of 200 atoms). For the evaluation of the third-order anharmonic interatomic force constants, we consider interactions up to the eleventh nearest neighbours. In this case, by using the ShengBTE[60] package, we calculate the force constants using the MTP for 312 structures in a negligible time, which otherwise with DFT would require significant computational resources. On the basis of the MTP trained over AIMD simulations within

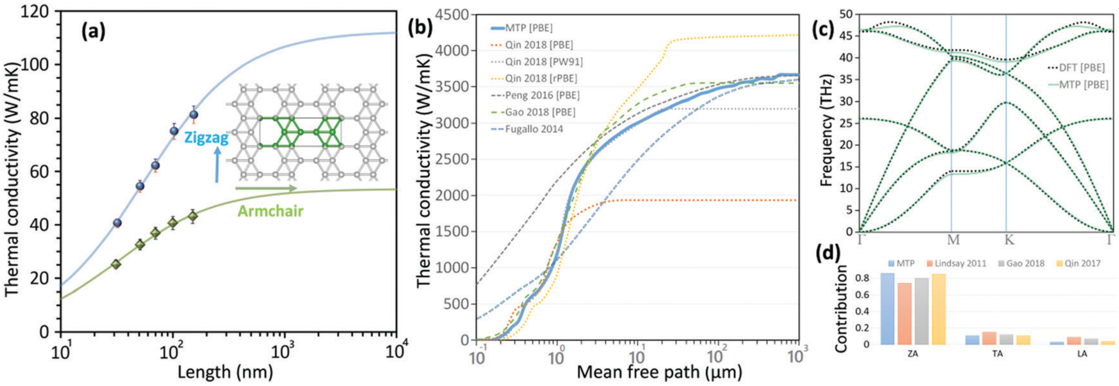

Fig. 3 (a) NEMD estimations for the length effect on the room temperature lattice thermal conductivity of single-layer borophene along the armchair and zigzag directions (continuous lines illustrate the fits to the NEMD data points). (b) Cumulative lattice thermal conductivity of graphene at the room temperature as a function of mean free path by fully iterative solutions of the Boltzmann transport equation using the MTP (present study) and full-DFT solutions by Fugallo *et al.*,[54] Peng *et al.*,[55] Gao *et al.*[56] and Qin *et al.*[57] with different exchange correlation functions. (c) Phonon dispersion relation of graphene acquired by the DFT (dotted line) and MTP (continuous line). (d) Contribution of ZA, TA and LA acoustic modes on the total lattice thermal conductivity of graphene by MTP (present study) and previous studies by Lindsay *et al.*,[58] Gao *et al.*[56] and Qin *et al.*[59]

the PBE/GGA functional, the diffusive lattice thermal conductivity of graphene is finally estimated to be 3600 W mK^{-1}, which falls within the experimentally measured values of 1500–5300 W mK^{-1}.[28–31] In Fig. 3b the cumulative lattice thermal conductivity of single-layer graphene as a function of mean free path using the MTP-based solution is compared with the existing full-DFT calculations, which show close trends. We note that depending on the type of exchange–correlation functional, as well as the chosen supercell size and cut-off distance, the obtained thermal conductivity of graphene varies substantially which explains the remarkable scattering in the available literature data. On the basis of PBE/GGA functional and using the ShengBTE package, the thermal conductivity of monolayer graphene at room temperature are predicted to be 1936,[57] 3100,[61] 3550,[62] 3845,[63] 3720,[55] 3288[64] and 5500 W mK^{-1}.[65] In Table S2 (ESI†), a more elaborated comparison with different experimental and full-DFT theoretical works on the thermal conductivity of single-layer graphene is achieved, which confirms the accuracy of the accelerated approach in this work. In Fig. 3c the phonon dispersion relations of graphene predicted by the DFT- and MTP-based methods show a close agreement (see Section 1.5 of the ESI,† for computational details). As it is well known, acoustic phonons are the main heat carriers in the graphene. Fig. 3d shows the good agreement for the contribution of different acoustic modes to the overall thermal conductivity of graphene using the MTP-based approach and full-DFT calculations.[56,58,59] In Fig. S3 (ESI†), the contribution of ZA, TA, LA and optical modes on the phonon's group velocity, scattering rate and Grüneisen parameter of single-layer graphene are also illustrated, and again show consistency with the existing full-DFT results. We further examine the validity of the proposed MTP-based method in predicting the lattice thermal conductivity, by considering the bulk silicon and InAs (see Section 7 of the ESI,† for computational details). The acquired results shown in Fig. S4 (ESI†) reveal close agreement between the proposed MTP-based approach and existing experimental and full-DFT studies. Our results thus confirm that MTP potentials can be effectively used to estimate the lattice thermal conductivity, not only by classical NEMD simulations but also with the full-iterative solution of the Boltzmann transport equation. In the latter case, the MTP-based approach can yield accurate results but with substantially reduced computational cost of the evaluation of anharmonic interatomic force constants in comparison with commonly employed DFT-based solution, which is a highly promising finding.

At this stage, we are capable to explore the effective lattice thermal conductivity of graphene/borophene heterostructures by employing the FEM simulations, in which we employ ABAQUS/Standard along with python scripting. For the construction of heterostructures, we develop polycrystalline samples made of 5000 individual grains on the basis of Voronoi cells with mirror symmetry at all edges.[66] Different grains are randomly assigned to be either graphene or borophene, according to the composition of heterostructures, simply by defining the corresponding thermal conductivity values acquired in the previous section. Since the borophene exhibits an anisotropic thermal transport, for the corresponding cells the anisotropic thermal conductivity tensors are defined by randomly selecting the orientation. The NEMD results for the thermal conductance of graphene/borophene grain boundaries are randomly chosen to introduce the interfacial conductance of every line connecting dissimilar crystals, and assuming perfect bonding (infinite conductance) for the rest of interfaces. To systematically investigate the size effect, we assume the equivalent grain size of the original polycrystalline sample as the domain size, assuming a square geometry for the equivalent average grain size.[66] A sample of heterostructure composition with 60% and 40% content of graphene and borophene phases, respectively, is shown in Fig. 4a. For the loading condition, we attach two highly conductive strips to the constructed sample and apply heat-fluxes (h_f) of the same magnitude on the outer surfaces of the two strips, one inward flux and one outward flux. As the initial value for the problem, the temperature of the outer surface of the cold strip (with outward flux) is set to zero.

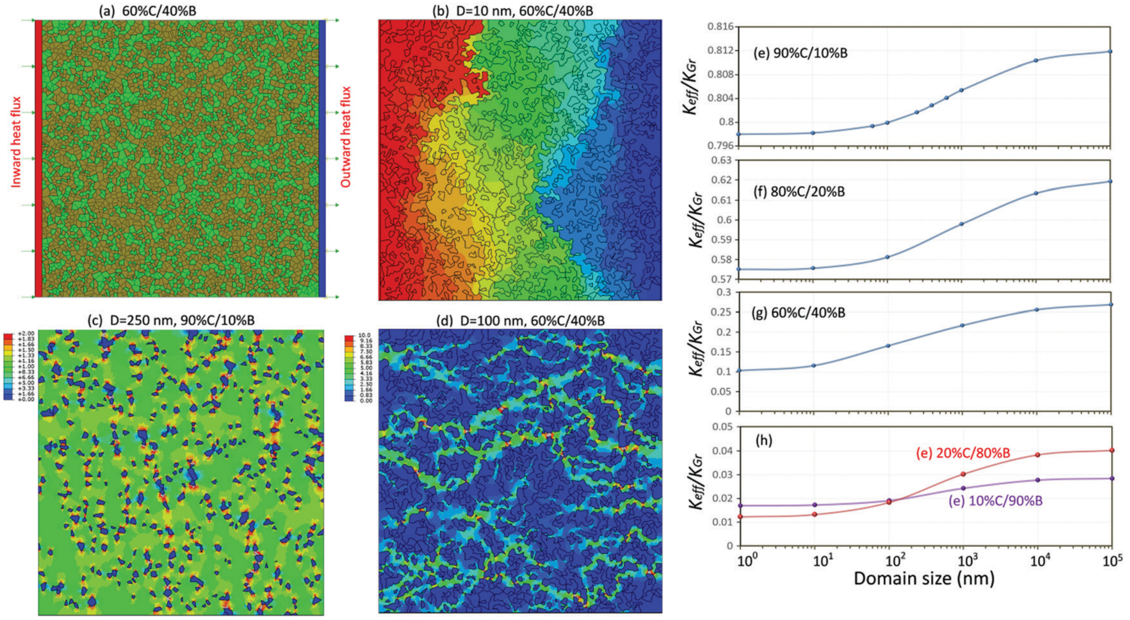

Fig. 4 (a) A samples of constructed continuum model of graphene/borophene heterostructure with 40% content of borophene crystals to evaluate the effective lattice thermal conductivity of polycrystalline graphene structures, (b) established steady-state temperature profile for the same sample with domain sizes of 10 nm. (c and d) Samples of heat flux distributions. (e–h) Normalized effective lattice thermal conductivity of heterostructure with respect to the graphene's thermal conductivity.

By solving the steady-state heat transfer problem, as shown in Fig. 4b a temperature profile establishes along the loading direction, which can be used to evaluate the effective thermal conductivity.[66] As expected and indeed observed in Fig. 4b–d, due to the high contrast in thermal conductivity of graphene and borophene, the temperature and heat flux profiles exhibit highly non-uniform distributions. This implies that the majority of heat fluxes are carried out *via* the percolation networks made of graphene crystals. To provide a more comprehensive vision on the heat transfer mechanism, we examine the effective lattice thermal conductivity for five different heterostructures and for domain sizes ranging from 1 nm to 100 μm (see Fig. 4e–h). It is clear that for all samples with extremely large domain sizes around 100 μm, the effective thermal conductivity is not yet fully converged, revealing the importance of assuming the interfacial thermal conductance for the modelling of thermal transport in these heterostructures. The presented results reveal three main behaviours of the effective thermal conductivity with respect to the domain size. Then first one occurring for domain sizes below 10 nm, the lattice thermal conductivity stays almost insensitive with respect to the domain size. This observation reveals that due to the presence of interfacial resistances, the embedded phases basically do not contribute to the heat flux transfer and exhibit a void like behaviour. This issue is noticeable when comparing the thermal conductivity of heterostructures with 10% and 20% content of graphene nanosheets (find Fig. 4h), in which the sample with the higher content of the ultrahigh conductive crystals yields lower conductivity for domain sizes lower than 100 nm. The second type of behaviour occurs for domain sizes from 10 nm to 10 μm, in which the thermal conductivity slowly increases with domain size. Such a trend implies that the effect of interfacial resistance starts to decline by increasing the domain size. If one considers for instance the sample with 10% content of borophene with a relatively large domain size of 250 nm, as seen in Fig. 4c, the borophene crystal contributes marginally to the heat flux transfer. For the sample with 40% content of borophene, it is noticeable that the majority of heat flux is transferred by graphene networks percolating each other (find Fig. 4d). In this case, borophene crystals not only participate marginally in the heat transfer but also impede thermal transport within the highly conductive graphene grains. In the third and last step, which dominates the thermal transport for domain sizes larger than 10 μm, the thermal conductivity reaches a plateau and only slightly increases by a further increase of the domain size, which reveals that the effect of interfacial resistance starts to vanish. From a practical point of view, this second step of heat transfer would be more close to real experimental samples, because it is normally very difficult to make heterostructures with domain sizes larger than 0.01 cm. Our results for domain sizes from 10 nm to 10 μm highlight that within these domain sizes, the interfacial thermal resistance plays the critical role and therefore should be taken into consideration. We would like to also clearly remind that in this study we mainly studied the lattice thermal conductivity, which may not be exactly the same as the total thermal conductivity, in which electrons contributions to the thermal conductivity are also taken into account.

Conclusion

In conclusion, our study confirms that machine-learning interatomic potentials trained over short *ab initio* molecular dynamics trajectories enable efficient first-principles multiscale modeling *via* hierarchical employment of density functional theory/classical molecular dynamics/finite element simulations. In other words, it is possible to examine the properties and responses of novel complex microstructures, without prior knowledge of properties of building blocks. To show this novel possibility, we explored the lattice thermal conductivity of graphene/borophene heterostructures, a system that to the best of our knowledge there exist no viable classical modeling alternative. Furthermore, it is shown that the developed machine-learning interatomic potentials can be effectively employed to acquire the lattice thermal conductivity not only by classical molecular dynamics simulations but also with the full-iterative solution of the Boltzmann transport equation. First-principles multiscale modeling is believed to offer novel and computationally efficient possibilities to evaluate the properties and improve the design of advanced nanostructured materials.

Methods

First-principles DFT calculations in this work were carried out using the Vienna Ab initio Simulation Package (VASP).[67–69] The generalized gradient approximation (GGA) and Perdew–Burke–Ernzerhof (PBE)[70] functional was adopted in the calculations. We assumed a plane-wave cutoff energy of 500 eV in our simulations. The phonon dispersion and second-order force constants of graphene were obtained by density functional perturbation theory (DFPT) simulations over a $10 \times 10 \times 1$ supercell sample using a $3 \times 3 \times 1$ Monkhorst-Pack[71] k-point grid along with the PHONOPY code.[72] *Ab initio* molecular dynamics (AIMD) simulations were performed with a time step of 1 fs using a $3 \times 3 \times 1$ k-point gird. For elaborated computational details, please refer to the supporting information document and the public Mendeley dataset of http://dx.doi.org/10.17632/pbgscy3ptg.1.

Conflicts of interest

There are no conflicts to declare.

Acknowledgements

B. M. and X. Z. appreciate the funding by the Deutsche Forschungsgemeinschaft (DFG, German Research Foundation) under Germany's Excellence Strategy within the Cluster of Excellence PhoenixD (EXC 2122, Project ID 390833453). E. V. P and A. V. S. were supported by the Russian Science Foundation (Grant No. 18-13-00479). ICN2 is supported by the Severo Ochoa program from Spanish MINECO (Grant No. SEV-2017-0706) and funded by the CERCA Programme/Generalitat de Catalunya.

References

1 N. Mounet, *et al.*, Two-dimensional materials from high-throughput computational exfoliation of experimentally known compounds, *Nat. Nanotechnol.*, 2018, **13**, 246–252.

2 A. R. Oganov and C. W. Glass, Crystal structure prediction using ab initio evolutionary techniques: principles and applications, *J. Chem. Phys.*, 2006, **124**, 244704.

3 A. R. Oganov, A. O. Lyakhov and M. Valle, How evolutionary crystal structure prediction works-and why, *Acc. Chem. Res.*, 2011, **44**, 227–237.

4 A. J. Mannix, *et al.*, Synthesis of borophenes: anisotropic, two-dimensional boron polymorphs, *Science*, 2015, **350**, 1513–1516.

5 B. Feng, *et al.*, Experimental Realization of Two-Dimensional Boron Sheets, *Nat. Chem.*, 2016, **8**, 563–568.

6 X. F. Zhou, *et al.*, Semimetallic two-dimensional boron allotrope with massless Dirac fermions, *Phys. Rev. Lett.*, 2014, **112**, 085502.

7 Z. Zhang, Y. Yang, G. Gao and B. I. Yakobson, Two-Dimensional Boron Monolayers Mediated by Metal Substrates, *Angew. Chem.*, 2015, **127**, 13214–13218.

8 C.-T. Toh, *et al.*, Synthesis and properties of free-standing monolayer amorphous carbon, *Nature*, 2020, **577**, 199–203.

9 B. Sun and A. S. Barnard, Visualising multi-dimensional structure/property relationships with machine learning, *J. Phys. Mater.*, 2019, **2**, 34003.

10 H. Oda, S. Kiyohara and T. Mizoguchi, Machine learning for structure determination and investigating the structure-property relationships of interfaces, *J. Phys. Mater.*, 2019, **2**, 34005.

11 G. R. Schleder, A. C. M. Padilha, C. M. Acosta, M. Costa and A. Fazzio, From DFT to machine learning: recent approaches to materials science-a review, *J. Phys. Mater.*, 2019, **2**, 32001.

12 J. Schmidt, M. R. G. Marques, S. Botti and M. A. L. Marques, Recent advances and applications of machine learning in solid-state materials science, *npj Comput. Mater.*, 2019, **5**, 83.

13 A. R. Oganov, C. J. Pickard, Q. Zhu and R. J. Needs, Structure prediction drives materials discovery, *Nat. Rev. Mater.*, 2019, **4**, 331–348.

14 I. A. Kruglov, *et al.*, Machine Learning Interatomic Potentials for Global Optimization and Molecular Dynamics Simulation, *Mater. Inf.*, 2019, 253–288, DOI: 10.1002/9783527802265.ch9.

15 Y. Liu, T. Zhao, W. Ju and S. Shi, Materials discovery and design using machine learning, *J. Mater*, 2017, **3**, 159–177.

16 P. C. Jennings, S. Lysgaard, J. S. Hummelshøj, T. Vegge and T. Bligaard, Genetic algorithms for computational materials discovery accelerated by machine learning, *npj Comput. Mater.*, 2019, **5**, 46.

17 P. Mikulskis, M. R. Alexander and D. A. Winkler, Toward Interpretable Machine Learning Models for Materials Discovery, *Adv. Intell. Syst*, 2019, **1**, 1900045.

18 C. Suh, C. Fare, J. A. Warren and E. O. Pyzer-Knapp, Evolving the Materials Genome: How Machine Learning Is Fueling the Next Generation of Materials Discovery, *Annu. Rev. Mater. Res.*, 2020, DOI: 10.1146/annurev-matsci-082019-105100.

19 Q. Zhou, *et al.*, Learning atoms for materials discovery, *Proc. Natl. Acad. Sci. U. S. A.*, 2018, **115**, E6411LP–E6417.

20 K. Gubaev, E. V. Podryabinkin, G. L. W. Hart and A. V. Shapeev, Accelerating high-throughput searches for new alloys with active learning of interatomic potentials, *Comput. Mater. Sci.*, 2019, **156**, 148–156.

21 E. V. Podryabinkin, E. V. Tikhonov, A. V. Shapeev and A. R. Oganov, Accelerating crystal structure prediction by machine-learning interatomic potentials with active learning, *Phys. Rev. B*, 2019, **99**, 064114.

22 V. V. Ladygin, P. Y. Korotaev, A. V. Yanilkin and A. V. Shapeev, Lattice dynamics simulation using machine learning interatomic potentials, *Comput. Mater. Sci.*, 2020, **172**, 109333.

23 I. S. Novikov and A. V. Shapeev, Improving accuracy of interatomic potentials: more physics or more data? A case study of silica, *Mater. Today Commun*, 2019, **18**, 74–80.

24 P. Korotaev, I. Novoselov, A. Yanilkin and A. Shapeev, Accessing thermal conductivity of complex compounds by machine learning interatomic potentials, *Phys. Rev. B*, 2019, **100**, 144308.

25 B. Mortazavi, *et al.*, Efficient machine-learning based interatomic potentials for exploring thermal conductivity in two-dimensional materials, *J. Phys. Mater.*, 2020, **3**, 02LT02.

26 E. V. Podryabinkin and A. V. Shapeev, Active learning of linearly parametrized interatomic potentials, *Comput. Mater. Sci.*, 2017, **140**, 171–180.

27 X. Liu and M. C. Hersam, Borophene-graphene heterostructures, *Sci. Adv.*, 2019, **5**, eaax6444.

28 S. Ghosh, *et al.*, Extremely high thermal conductivity of graphene: prospects for thermal management applications in nanoelectronic circuits, *Appl. Phys. Lett.*, 2008, **92**, 1–4.

29 A. A. Balandin, *et al.*, Superior thermal conductivity of single-layer graphene, *Nano Lett.*, 2008, **8**, 902–907.

30 L. A. Jauregui, *et al.*, Thermal Transport in Graphene, *Nanostructures: Experiments and Simulations*, 2010, **28**, 73–83.

31 W. Cai, *et al.*, Thermal transport in suspended and supported monolayer graphene grown by chemical vapor deposition, *Nano Lett.*, 2010, **10**, 1645–1651.

32 J. Tersoff, Modeling solid-state chemistry: interatomic potentials for multicomponent systems, *Phys. Rev. B: Condens. Matter Mater. Phys.*, 1989, **39**, 5566–5568.

33 S. J. Stuart, A. B. Tutein and J. A. Harrison, A reactive potential for hydrocarbons with intermolecular interactions, *J. Chem. Phys.*, 2000, **112**, 6472–6486.

34 D. W. Brenner, *et al.*, A second-generation reactive empirical bond order (REBO) potential energy expression for hydrocarbons, *J. Phys.: Condens. Matter*, 2002, **14**, 783, DOI: 10.1088/0953-8984/14/4/312.

35 L. Lindsay and D. A. Broido, Optimized Tersoff and Brenner empirical potential parameters for lattice dynamics and phonon thermal transport in carbon nanotubes and graphene, *Phys. Rev. B: Condens. Matter Mater. Phys.*, 2010, **81**, 205441.

36 Z. Wei, Z. Ni, K. Bi, M. Chen and Y. Chen, In-plane lattice thermal conductivities of multilayer graphene films, *Carbon N. Y.*, 2011, **49**, 2653–2658.

37 Y. Hong, M. G. Ju, J. Zhang and X. C. Zeng, Phonon thermal transport in a graphene/MoSe2 van der Waals heterobilayer, *Phys. Chem. Chem. Phys.*, 2018, **20**, 2637–2645.

38 J. A. Thomas, R. M. Iutzi and A. J. H. McGaughey, Thermal conductivity and phonon transport in empty and water-filled carbon nanotubes, *Phys. Rev. B: Condens. Matter Mater. Phys.*, 2010, **81**, 045413.

39 B. Mortazavi and T. Rabczuk, Multiscale modeling of heat conduction in graphene laminates, *Carbon N. Y.*, 2015, **85**, 1–7.

40 Z. Fan, *et al.*, Thermal conductivity decomposition in two-dimensional materials: application to graphene, *Phys. Rev. B*, 2017, **95**, 144309.

41 S. M. Hatam-Lee, A. Rajabpour and S. Volz, Thermal conductivity of graphene polymorphs and compounds: from C3N to graphdiyne lattices, *Carbon N. Y.*, 2020, **161**, 816–826.

42 M. Raeisi, S. Ahmadi and A. Rajabpour, Modulated thermal conductivity of 2D hexagonal boron arsenide: a strain engineering study, *Nanoscale*, 2019, **11**, 21799–21810.

43 S. Bazrafshan and A. Rajabpour, Engineering of thermal transport in graphene using grain size, strain, nitrogen and boron doping; a multiscale modeling, *Int. J. Heat Mass Transfer*, 2018, **123**, 534–543.

44 A. V. Shapeev, Moment tensor potentials: a class of systematically improvable interatomic potentials, *Multiscale Model. Simul.*, 2016, **14**, 1153–1173.

45 Y. Liu and B. I. Yakobson, Cones, pringles, and grain boundary landscapes in graphene topology, *Nano Lett.*, 2010, **10**, 2178–2183, DOI: 10.1021/nl100988r.

46 A. M. van der Zande, *et al.*, Grains and grain boundaries in highly crystalline monolayer molybdenum disulphide, *Nat. Mater.*, 2013, **12**, 554–561.

47 S. Najmaei, *et al.*, Vapour phase growth and grain boundary structure of molybdenum disulphide atomic layers, *Nat. Mater.*, 2013, **12**, 754–759.

48 W. Zhou, *et al.*, Intrinsic structural defects in monolayer molybdenum disulfide, *Nano Lett.*, 2013, **13**, 2615–2622.

49 S. Plimpton, Fast Parallel Algorithms for Short-Range Molecular Dynamics, *J. Comput. Phys.*, 1995, **117**, 1–19.

50 B. Mortazavi, *et al.*, Strong thermal transport along polycrystalline transition metal dichalcogenides revealed by multiscale modeling for MoS_2, *Appl. Mater. Today*, 2017, **7**, 67–76.

51 J. E. Barrios-Vargas, *et al.*, Electrical and Thermal Transport in Coplanar Polycrystalline Graphene-hBN Heterostructures, *Nano Lett.*, 2017, **17**, 1660–1664.

52 P. K. Schelling, S. R. Phillpot and P. Keblinski, Comparison of atomic-level simulation methods for computing thermal conductivity, *Phys. Rev. B: Condens. Matter Mater. Phys.*, 2002, **65**, 1–12.

53 X. Zhang, *et al.*, Thermal conductivity of silicene calculated using an optimized Stillinger-Weber potential, *Phys. Rev. B: Condens. Matter Mater. Phys.*, 2014, **89**, 054310.

54 G. Fugallo, *et al.*, Thermal conductivity of graphene and graphite: collective excitations and mean free paths, *Nano Lett.*, 2014, **14**, 6109–6114.

55 B. Peng, *et al.*, Phonon transport properties of two-dimensional group-IV materials from ab initio calculations, *Phys. Rev. B*, 2016, **94**, 245420.

56 Y. Gao, *et al.*, First-principles study of intrinsic phononic thermal transport in monolayer C3N. *Phys. E Low-dimensional Syst, Nanostructures*, 2018, **99**, 194–201.

57 G. Qin, Z. Qin, H. Wang and M. Hu, On the diversity in the thermal transport properties of graphene: a first-principles-benchmark study testing different exchange-correlation

functionals, *Comput. Mater. Sci.*, 2018, **151**, 153–159, DOI: 10.1016/j.commatsci.2018.05.007.

58 L. Lindsay, D. A. Broido and N. Mingo, Flexural phonons and thermal transport in multilayer graphene and graphite, *Phys. Rev. B: Condens. Matter Mater. Phys.*, 2011, **83**, 235428.

59 Z. Qin, G. Qin, X. Zuo, Z. Xiong and M. Hu, Orbitally driven low thermal conductivity of monolayer gallium nitride (GaN) with planar honeycomb structure: a comparative study, *Nanoscale*, 2017, **9**, 4295–4309.

60 W. Li, J. Carrete, N. A. Katcho and N. Mingo, ShengBTE: a solver of the Boltzmann transport equation for phonons, *Comput. Phys. Commun.*, 2014, **185**, 1747–1758.

61 H. Wang, *et al.*, Lone-Pair Electrons Do Not Necessarily Lead to Low Lattice Thermal Conductivity: An Exception of Two-Dimensional Penta-CN2, *J. Phys. Chem. Lett.*, 2018, **9**, 2474–2483.

62 Y. Gao, *et al.*, First-principles study of intrinsic phononic thermal transport in monolayer C_3N. *Phys. E Low-dimensional Syst*, *Nanostructures*, 2018, **99**, 194–201.

63 X. Tan, *et al.*, High thermoelectric performance in two-dimensional graphyne sheets predicted by first-principles calculations, *Phys. Chem. Chem. Phys.*, 2015, **17**, 22872–22881.

64 L. Lindsay, *et al.*, Phonon thermal transport in strained and unstrained graphene from first principles, *Phys. Rev. B: Condens. Matter Mater. Phys.*, 2014, **89**, 155426.

65 A. Taheri, C. Da Silva and C. H. Amon, First-principles phonon thermal transport in graphene: effects of exchange–correlation and type of pseudopotential, *J. Appl. Phys.*, 2018, **123**, 215105.

66 B. Mortazavi, M. Pötschke and G. Cuniberti, Multiscale modeling of thermal conductivity of polycrystalline graphene sheets, *Nanoscale*, 2014, **6**, 3344–3352.

67 G. Kresse and J. Furthmüller, Efficiency of *ab initio* total energy calculations for metals and semiconductors using a plane-wave basis set, *Comput. Mater. Sci.*, 1996, **6**, 15–50.

68 G. Kresse and J. Furthmüller, Efficient iterative schemes for ab initio total-energy calculations using a plane-wave basis set, *Phys. Rev. B: Condens. Matter Mater. Phys.*, 1996, **54**, 11169–11186.

69 G. Kresse, From ultrasoft pseudopotentials to the projector augmented-wave method, *Phys. Rev. B: Condens. Matter Mater. Phys.*, 1999, **59**, 1758–1775.

70 J. Perdew, K. Burke and M. Ernzerhof, Generalized Gradient Approximation Made Simple, *Phys. Rev. Lett.*, 1996, **77**, 3865–3868.

71 H. Monkhorst and J. Pack, Special points for Brillouin zone integrations, *Phys. Rev. B: Condens. Matter Mater. Phys.*, 1976, **13**, 5188–5192.

72 A. Togo and I. Tanaka, First principles phonon calculations in materials science, *Scr. Mater.*, 2015, **108**, 1–5.